Scientific Research Publishing

Open Journal of Applied Sciences, 2026, 16(1), 48-68
https://www.scirp.org/journal/ojapps
ISSN Online: 2165-3925
ISSN Print: 2165-3917

An Explainable Wavelet-Based Feature Decomposition and Machine Learning Framework for Land Cover Classification

Saviour Mantey[1], Richmond Akwasi Nsiah[1], Maame Boama Poku[2]

[1]Department of Geomatic Engineering, University of Mines and Technology, Tarkwa, Ghana
[2]Department of Geomatic and Civil Engineering, University of Mines and Technology, Essikado, Ghana
Email: smantey@umat.edu.gh, ransiah@umat.edu.gh, mbpoku@umat.edu.gh

How to cite this paper: Mantey, S., Nsiah, R.A. and Poku, M.B. (2026) An Explainable Wavelet-Based Feature Decomposition and Machine Learning Framework for Land Cover Classification. *Open Journal of Applied Sciences*, **16**, 48-68.
https://doi.org/10.4236/ojapps.2026.161005

Received: December 11, 2025
Accepted: January 1, 2026
Published: January 4, 2026

Abstract

Accurate land cover classification is essential for environmental monitoring, urban planning, and resource management. Conventional classifiers trained on raw spectral bands are often limited by noise, inter-class spectral similarity, and intra-class variability. This study introduces a wavelet-based feature decomposition and machine learning framework to address these challenges. Landsat-8 Operational Land Imager (OLI) Level-2 surface reflectance data were pre-processed and decomposed using a one-dimensional discrete wavelet transform to isolate low- and high-frequency components. The decomposed features were concatenated with raw bands to form an enriched dataset, which was used to train and validate three supervised classifiers: Random Forest (RF), Gradient Boosting (GBM), and Decision Tree (DT). Model performance was evaluated using 5-fold cross-validation, and the best-performing model, the Random Forest Wavelet Transform (RF_WT), achieved the highest macro-F1 score (0.865). Explainable AI (Gini importance, permutation importance, SHAP (SHapley Additive exPlanations) values) confirmed the complementary role of raw and decomposed features, with wavelet-derived detail components in the Short-Wave Infrared (SWIR) and visible bands strongly influencing classification. The RF_WT model, when compared to RF, DT and GBM classifiers trained on raw spectral bands across all classes, achieved the highest macro-averaged accuracy values (UA = 0.876, PA = 0.864, F1 = 0.865), compared with RF (UA = 0.864, PA = 0.852, F1 = 0.853), GBM (UA = 0.849, PA = 0.832, F1 = 0.832), and DT (UA = 0.815, PA = 0.808, F1 = 0.809). The approach is valuable in support of ecological monitoring and resource management. However, challenges in settlement classification highlight the limitations of medium-resolution data. Future work could integrate higher-resolution imagery or multi-temporal data for improved performance.

Keywords

Land Cover, Machine Learning, Wavelet Transform, Classification, Explainable AI (xAI)

1. Introduction

Land cover refers to the physical materials at Earth's surface, including vegetation, urban infrastructure, water bodies, and bare soil [1] [2]. Accurate land cover classification is essential for various applications, including environmental monitoring, urban planning, and natural resource management [3]-[5]. Moreover, accurately classifying land cover provides critical information on the distribution and changes of land surfaces over time [6]. Traditionally, land cover data has been obtained through two primary approaches: terrestrial surveys and remote sensing using satellite or aerial imagery [7]. While terrestrial surveys offer high precision and detail, they are labour-intensive, time-consuming, and often impractical for large or inaccessible areas [8]. In contrast, remote sensing methods provide extensive spatial coverage and multi-temporal data, making them a cost-effective alternative for land cover mapping [7].

One of the most widely used methods for land cover classification in remote sensing is the pixel-based approach, which analyses the spectral information of individual pixels in satellite or aerial images [6] [9]. The pixel-based approach is favoured for its ability to utilise the rich spectral data provided by remote sensors, enabling the classification of various land cover types based on their unique spectral [10]. This approach can be implemented using both supervised and unsupervised classification techniques [11]. In unsupervised classification, algorithms such as ISO-cluster, Self-Organising Map (SOM) networks, and K-means clustering group pixels into clusters based on spectral similarities without requiring labelled training data [1] [2]. While unsupervised classification is advantageous when labelled data is scarce or unavailable, it often results in less accurate classifications and necessitates post-classification refinement techniques and prior masking [12].

In contrast, supervised classification tends to produce more accurate results as it leverages prior knowledge from labelled data to guide the classification process [2] [13]. Despite requiring a substantial amount of labelled data and being more computationally intensive, the supervised approach is generally preferred for land cover classification [12] [14]. In supervised classification, statistical algorithms such as Maximum Likelihood Classification (MLC) or Machine Learning (ML) algorithms such as Support Vector Machines (SVM), Random Forests (RF), and Decision Tree (DT), among others [1] [7], are trained on labelled data to identify and classify land cover types in new images. Statistical algorithms classify pixels based on probability distributions, but they are limited by their reliance on statistical parameters and assumptions about pixel value distributions [12]. ML algo-

rithms are more adaptable and flexible alternatives to address these limitations. Unlike statistical methods, ML algorithms can autonomously learn complex patterns from labelled training data and apply this knowledge to classify new data, making them particularly valuable for urban land cover mapping [15]. Despite these advancements, utilising ML for classification presents several other significant obstacles. These include noise and artefacts in satellite images, which can distort spectral information and lead to misclassification [16]. Furthermore, spectral similarity across land cover classes often hampers ML algorithms' ability to accurately distinguish between them. Intra-class variability adds another layer of complexity, as the diverse characteristics within a single land cover type can make it difficult for ML classifiers to learn and generalise consistent patterns [5] [15] [17] [18]. As a unit, these challenges can severely impact the accuracy and reliability of ML-based land cover classifications.

Over the past decade, significant progress has been made in overcoming these limitations in Hyperspectral Image (HSI) through spectral-spatial feature decomposition techniques, particularly Singular Spectrum Analysis (SSA) and its variants. For example, [19] proposed using 2D-SSA for spatial feature extraction, emphasising its ability to decompose HSI data into varying trends and oscillations. The method demonstrated superior performance in suppressing noise and enhancing the discriminative power of the extracted features. Similarly, [20] explored a multiscale 2D-SSA-based feature fusion method combined with Segmented Principal Component Analysis (SPCA) to enhance the extraction of both spectral and spatial features. The approach effectively decomposes HSI data into multiple components, capturing trends and oscillations while suppressing noise, thereby improving classification accuracy. The integration of SPCA further refines the dimensionality reduction, making the feature extraction process more robust and computationally efficient. [16] introduced a SPCA-based multiscale 2D-SSA fusion method that jointly leverages the strengths of spectral and spatial-domain feature extraction. The method successfully fuses these features by applying SPCA for initial dimensionality reduction, followed by 2D-SSA for multiscale spatial feature extraction, resulting in a comprehensive spectral-spatial feature set. This approach demonstrated superior performance across several benchmark HSI datasets, particularly in scenarios with limited training samples. [21] further expanded on this concept by integrating Principal Components Analysis (PCA) with edge-preserving filtering within a visualisation framework for HSIs. This method decomposes images into base and detail layers, with PCA applied to the base layers for global feature extraction. The approach not only preserves large-scale boundary information but also enhances mid- and small-scale textures, thereby improving image contrast and detail preservation in the visualisation of HSIs.

The previous articles demonstrate that feature decomposition methods have proven highly effective in hyperspectral image analysis. To the best of the authors' knowledge, no previous study has adapted signal-decomposition principles to the

spectral domain of multispectral pixels. Applying these techniques to multispectral imagery, such as Landsat-8, presents distinct challenges. Compared with hyperspectral images, which form a near-continuous, smooth spectral curve ideal for detailed frequency-based decomposition, multispectral sensors provide only a limited number of discrete broad bands, resulting in sparser sampling and shorter, step-like spectral vectors. This configuration risks losing subtle frequency components that decomposition aims to isolate, requiring careful selection of wavelet functions and decomposition levels to avoid under- or over-representation of frequencies. Consequently, the effectiveness of such methods on multispectral data cannot be assumed and remains largely unexplored.

This study addresses this gap by introducing a novel one-dimensional discrete wavelet transform (1D-DWT) applied directly to each pixel's spectral vector (treating the spectral bands as a 1D signal). Consequently, low-frequency trend components (representing the overall reflectance shape) are isolated from high-frequency detail and edge components (capturing abrupt spectral transitions and fine oscillatory behaviour) within the same pixel. The original spectral bands are then augmented by three physically interpretable wavelet reconstructions (full reconstruction, trend-only, and detail-only), yielding a compact yet enriched 24-feature set per pixel. The resulting feature set is used to train Random Forest (RF), Gradient Boosting Machine (GBM), and Decision Tree (DT) classifiers, with the best-performing wavelet-augmented model (RF_WT) further interpreted using multiple explainable AI (xAI) techniques (Gini importance, permutation importance, and SHAP values).

Thus, the research makes a novel contribution by adapting and applying a one-dimensional discrete wavelet transform (1D-DWT) to multispectral land cover classification. The main contributions of the study are:

- Novel Feature Engineering: Creating an enriched, interpretable feature set by decomposing each pixel's spectral signature into low-frequency trends and high-frequency details, then combining these with the original bands.
- Effective Model Development: Building and validating a wavelet-enhanced Random Forest model (RF_WT) that demonstrably outperforms standard classifiers on Landsat-8 data.
- Explainable Workflow: Using a multi-metric explainability framework to assess the contribution of the wavelet features to the model improvement.

2. Materials and Methods

2.1. Study Area

In this study, the Greater Accra Region, which houses Accra, the capital city of Ghana, was used as the study area (**Figure 1**). It is a rapidly urbanising area extending about 3 756.737 km^2 and lies between longitudes 0˚36'00"E and 0˚31'00"W and latitudes 5˚29'00"N and 6˚7'00"N. The land cover of the study area is a heterogeneous mix of natural and man-made features, comprising five main classes: water bodies, vegetation, forest, bare lands, and built-up areas or settlements [22].

The study area was covered by a single scene (path 196, row 054), although in Google Earth Engine (GEE), users do not specifically select the path and row of the scenes [23].

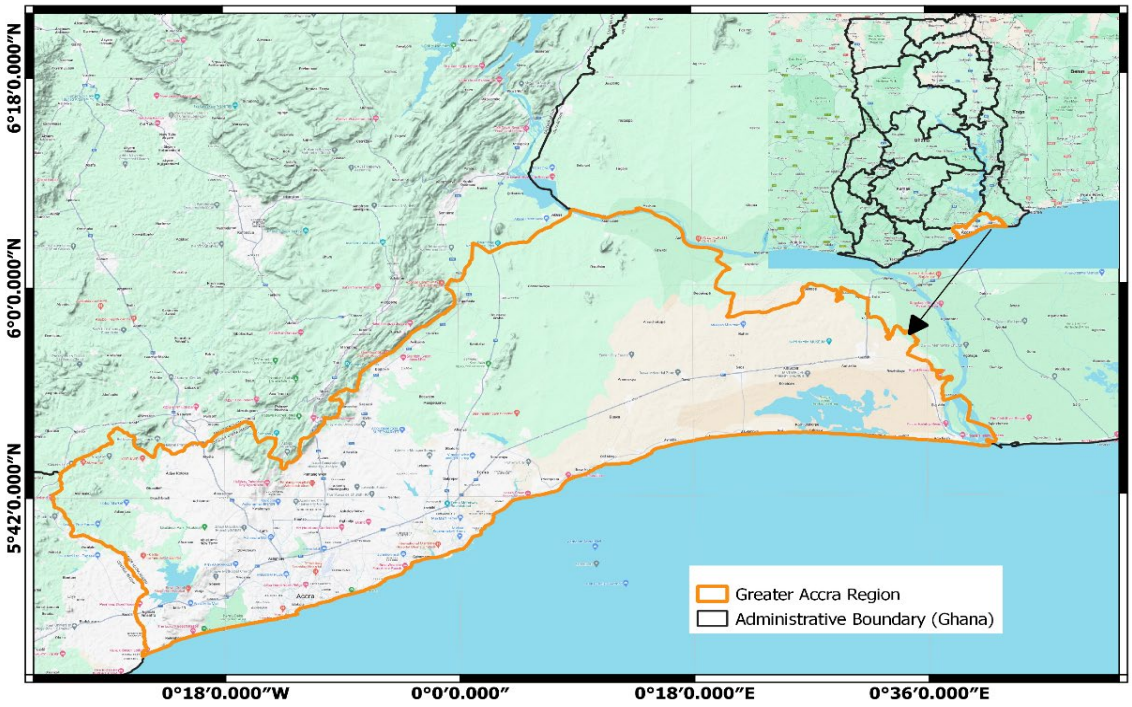

Figure 1. Study area: greater Accra region.

2.2. Methods

The methodological framework adopted for this study is illustrated in **Figure 2**. The workflow begins with data acquisition and preprocessing, followed by the

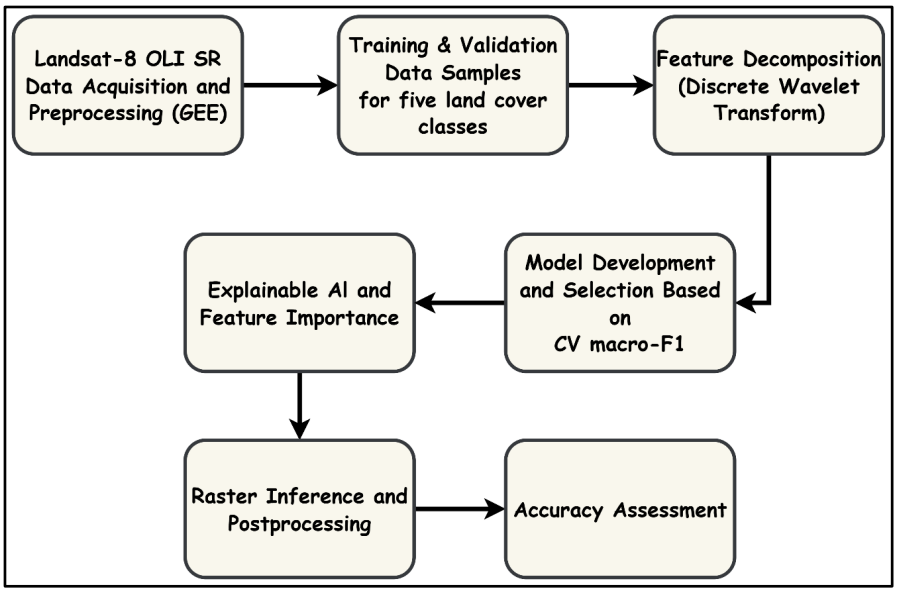

Figure 2. Methodological framework adopted for the study.

generation of training and validation samples, and then by wavelet-based decomposition of spectral vectors to construct an enriched feature set. Supervised classifiers (RF, GBM, DT) were trained and evaluated, with the best-performing model selected based on cross-validated macro-F1. Explainable AI techniques were then applied to assess feature contributions, after which the chosen model was deployed tile-wise to produce classified maps. Finally, post-processing and accuracy assessment were performed using a 3 × 3 majority filter and an independent validation set, respectively, to reduce salt-and-pepper noise and evaluate classification performance.

2.3. Dataset

This study utilised Landsat 8 Operational Land Imager (OLI) Level-2 Surface Reflectance (SR) data to perform land cover classification. The spatial resolution (30 meters) and frequent temporal coverage (16-day revisit period) of Landsat 8 make it ideal for monitoring land cover changes over time [24]. Landsat 8 OLI Level-2 products provide atmospherically corrected surface reflectance values, essential for accurate and consistent land cover analysis by minimising atmospheric distortions [25].

The data were accessed and processed using GEE, a cloud-based platform for large-scale geospatial analysis. GEE provides seamless access to this dataset, enabling efficient retrieval and processing without manual downloads [26]. Landsat 8 Level-2 SR data was accessed through the GEE platform by querying the LANDSAT/LC08/C01/T1_SR collection. The collection was filtered based on a vector file that defined the study area, a cloud cover percentage, and a date range. This step ensured that only relevant scenes within the specified boundaries were selected for analysis. Although Level-2 SR data includes some atmospheric corrections, additional cloud masking was performed using the Quality Assessment (QA) band provided in the dataset. The "pixel_qa" band was used to identify and mask clouds, cloud shadows, and other atmospheric artefacts. This step ensures that only clear-sky pixels are used in the subsequent analysis, thereby enhancing classification accuracy. Subsequently, a median composite of the cloud-masked images was generated. The median composite approach combines multiple images by taking the median value for each pixel, effectively mitigating the effects of residual clouds, reducing noise and improving the signal-to-noise ratio [26]. Relevant spectral bands necessary for land cover classification were selected from the composite image and stacked to form a multi-band image. The selected bands included the visible (Blue, Green, Red), near-infrared (NIR), and shortwave-infrared (SWIR) bands.

2.4. Training and Validation Samples

In the study area, five predominant land cover classes were identified: 1) bare land (BL), 2) forest (F), 3) vegetation (V), 4) settlements (S), and 5) water (W). Training and validation samples for these classes were randomly selected through man-

ual visual interpretation of high-resolution images from Google Earth, following methodologies employed in previous studies [27]-[31]. This process involved visually identifying and classifying land cover types based on expert interpretation of spectral and spatial characteristics observable in the imagery. A total of 2 189 samples were randomly sampled across the study area, and the reflectance values for each band corresponding to the identified land cover classes were extracted at each pixel. The distribution of samples used for training and validation was as follows: Bare land (144 samples), Forest (311 samples), Vegetation (424 samples), Settlements (1143 samples), and water (167 samples).

2.5. Data Decomposition and Reconstruction

This study employed the wavelet transform to decompose each spectral band into multiple frequency components. The wavelet transform is discussed in detail in [32]-[34]. In brief, the wavelet transform is a mathematical technique that decomposes a signal or a dataset into components of different frequencies. Unlike other approaches, such as the Fourier Transform, which decomposes a signal into sinusoidal waves, the wavelet transform uses "wavelets", which are small waves with finite duration, to analyse localised variations in the signal.

In this study, the pixels of the six-element spectral vector were treated as a one-dimensional signal using a discrete wavelet transform (Daubechies-2, level 1). The Daubechies-2 (db-2) was selected for its compact support and moderate smoothness, while the single-level (level-1) is capable of separating the approximations from the details (at higher decomposition levels, information is lost). This combination provided a trade-off between frequency localisation and computational efficiency without introducing redundancy, which is appropriate for the limited spectral resolution of Landsat-8 [35]. Subsequently, three reconstructions were generated: (i) "ALL" using all coefficients, (ii) "TREND" using only approximation coefficients, and (iii) "EDGE" using only detail coefficients. These reconstructions isolated low-frequency background structure and high-frequency edge- or texture-like variation in the spectral domain. The raw bands and their three reconstructions were concatenated to produce 24 interpretable features per pixel (RAW_B1…B6; WTALL_B1…B6; WTTR_B1…B6; WTED_B1…B6).

2.6. Model Development and Selection

Three machine learning classifiers, RF, DT, and GBM, were deployed using Python to model the resulting datasets. Decision Trees (DT) are a type of supervised learning algorithm introduced by [36] with his ID3 algorithm. A DT algorithm works by recursively splitting the data into subsets based on the value of input features. The goal is to create a tree where each internal node represents a decision rule based on a feature, and each leaf node represents an output label. Random Forest (RF) is an ensemble learning method introduced by [37] that uses bagging to create multiple subsets of the training data by sampling with replacement. Unlike DT, RF selects a random subset of features to determine the best split, thereby

reducing correlation among trees and increasing diversity within the ensemble [28]. Gradient Boosting Machines (GBM) is an ensemble learning technique introduced by [38]. GBM builds models sequentially, with each new model correcting errors from previous models. The algorithm sequentially adds weak learners (usually decision trees) to form a strong learner. Each tree is built to minimise the residual errors of the previous trees using a gradient descent-like procedure [39] [40]. The hyperparameters of each classifier were optimised via randomised grid search with stratified five-fold cross-validation, using macro-F1 as the selection metric to balance class performance. The classifier achieving the highest cross-validated macro-F1 score was retained for further analysis and raster inference. To ensure a robust comparison, all the baseline models (RF, DT and GBM) trained solely on raw spectral bands and were subjected to same hyperparameter optimisation strategy.

Although the dataset showed a notable class imbalance, no explicit class resampling or weighting techniques were applied during model training. Instead, the stratified five-fold cross-validation and macro-F1 were deemed sufficient as optimisation and selection metrics to mitigate the overshadowing of minority classes by the dominant settlement class. Moreover, this approach allowed each class to contribute equally to model evaluation and selection, while preserving the original data distribution and mitigating imbalance effects during evaluation.

2.7. Explainable AI (xAI)

This step was performed to enable transparency. As such, feature contributions to model performance were quantified through three importance metrics applied to an independent validation dataset. These included Gini, permutation importance and SHAP. Gini importance was used to capture the internal role of features in reducing node impurity during model training, providing a quick, model-internal diagnostic. Permutation importance was chosen as a model-agnostic metric to quantify each feature's contribution to generalisation by measuring the decrease in macro-F1 when feature values were randomly shuffled. Finally, SHAP values were employed to provide additive, game-theoretic insights into feature contributions at both global and local levels, allowing interpretation of both directionality and class-specific influences. For clarity in reporting, importances were exported both at the individual feature level and in aggregated form, grouped by feature "family" (RAW, WTALL, WTTR, WTED) and by band (B1…B6). This procedure enabled explicit identification of whether high-frequency wavelet details in specific spectral regions contributed more significantly to classification performance than raw band responses.

2.8. Map Production and Post-Processing

To ensure optimising memory usage, the selected model was applied to the cloud-masked median composite of the study areas using a tile-wise prediction routine (1024 × 1024 pixels). For each tile, the identical feature stack (RAW plus three

wavelet reconstructions) was reconstructed, and a 3 × 3 majority filter was applied to the classified map to reduce salt-and-pepper noise while preserving NoData values. Optionally, pixels with uncertainty values exceeding a defined threshold were masked as NoData prior to filtering, thereby preventing low-confidence predictions from being incorporated into the spatial smoothing. All post-processed outputs preserved the spatial resolution, georeferencing, and projection of the input composite.

2.9. Accuracy Assessment

The post-classification accuracy assessment employed was similar to that described by [28] and [41]. An equal stratified random sampling technique was used to generate 50 sample points for each land cover class. This approach helped assign similar weights to each class and ensured equal representativeness in the accuracy assessment. High-resolution imagery from Google Earth was used to visually inspect the samples.

For a 30 m × 30 m area, the dominant land cover type was determined and assigned to each sample. The accuracy of the land cover product was assessed by comparing reference samples with the classified data using a confusion matrix. From the confusion matrix, the producer's accuracy (recall), user's accuracy (precision), and F1-score were calculated for each land cover class, alongside overall and macro-averaged values. The confusion matrices were analysed alongside the xAI diagnostics to interpret classification errors and relate performance differences to specific feature families and spectral bands.

3. Results

In the proposed approach, each pixel's spectral vector was first decomposed using a one-dimensional discrete wavelet transform to isolate low-frequency trends and high-frequency detail components. The raw bands and their three wavelet reconstructions were then concatenated into a feature set, which was used to train the three supervised classifiers: RF_WT, DT_WT, and GBM_WT. Based on five-fold cross-validated macro-F1 scores, the RF model achieved the highest performance, with a mean macro-F1 of 0.865, and was therefore selected for detailed analysis and interpretation. Subsequently, the results presented in this section evaluate the performance of the Random Forest Wavelet Transform (RF_WT) model relative to baseline classifiers trained solely on raw spectral bands: Random Forest (RF), Decision Tree (DT), and Gradient Boosting Machine (GBM). To enhance interpretability, three explainable AI metrics, Gini importance, permutation importance, and SHAP values, were applied to RF_WT, and the ten most influential features are presented. These outputs provide insights into the relative contributions of raw and wavelet-derived features to land cover discrimination. Additionally, post-processing assessments are presented for the RF_WT and baseline models trained on the raw spectral bands. These include producer's accuracy (PA), user's accuracy (UA), and F1-scores for the independent validation dataset, as well

as the spatial outputs of the classification pipeline.

3.1. Feature Importance Analysis

The first ten most important features, as identified by Gini importance, permutation importance, and SHAP values, are presented in Tables 1-3 and Figure 3. Across the three methods, both raw and wavelet-derived features made substantial contributions to classification outcomes. Visible bands (B3, B4) consistently ranked highly, while wavelet-derived detail components (particularly WTED_B5 in SWIR1) were also strongly emphasised. SHAP values confirmed the complementary role of raw and decomposed features, showing that wavelet features enriched the spectral signal rather than replacing the raw bands.

Table 1. Feature importance (Gini).

Feature Name	Importance
family:RAW	0.311774188
family:WTALL	0.293209719
band:B3	0.276308687
family:WTED	0.234836718
band:B4	0.222869117
family:WTTR	0.160179376
band:B2	0.151140159
band:B1	0.124194361
feature:RAW_B3	0.124036126
band:B5	0.117522961
band:B6	0.107964714

Table 2. Feature importance (Permutation).

Feature Name	Importance
family:WTED	0.185997
feature:WTED_B5	0.14364
band:B5	0.140937
band:B1	0.035739
feature:WTED_B6	0.034783
band:B6	0.034538
feature:WTALL_B1	0.011654
feature:RAW_B1	0.010687
band:B2	0.010085

Table 3. Feature importance (SHAP Values).

Feature Name	Importance
family:RAW	0.614122
family:WTALL	0.584398
family:WTED	0.468395
band:B3	0.459507
band:B4	0.435883
family:WTTR	0.372987
band:B2	0.366286
band:B1	0.322165
band:B6	0.234545
band:B5	0.221515

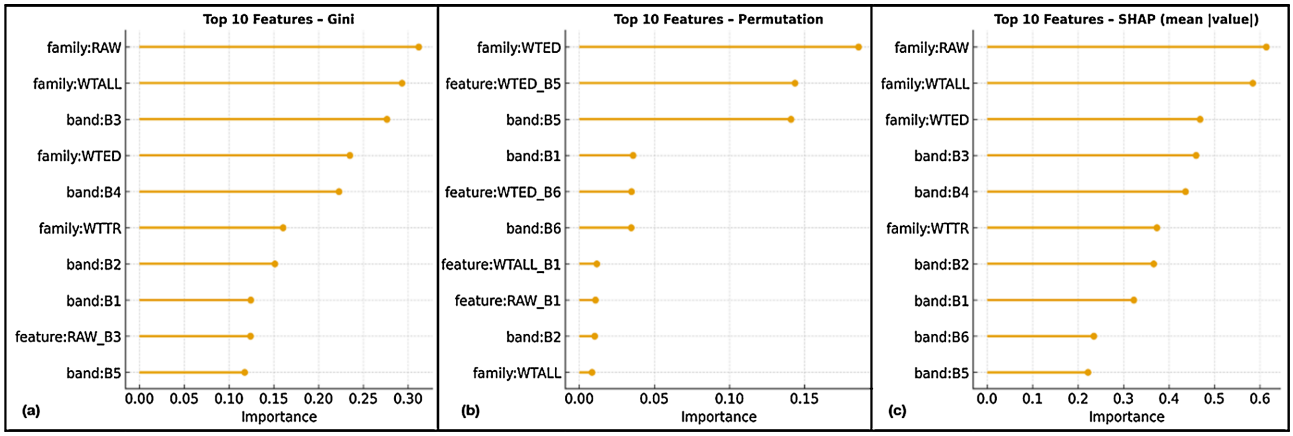

Figure 3. Feature importance based on (a) Gini (b) Permutation, and (c) SHAP values.

3.2. Classified Maps

Figure 4 presents the classified outputs from the four models. Among the four outputs, the RF_WT filtered map (**Figure 4(a)**) provided the most spatially coherent classification, with reduced salt-and-pepper noise and well-defined boundaries between vegetation and water. By contrast, the DT map (**Figure 4(b)**) exhibited fragmentation and scattered misclassifications, whereas the GBM map (Figure 3(c)) merged vegetation and settlements in heterogeneous areas. The baseline RF map (**Figure 4(d)**) was cleaner than DT and GBM but less spatially coherent than RF_WT. Generally, while the baseline models captured the general distribution of land cover classes, they exhibited more fragmented patterns, particularly in settlement and vegetation areas.

3.3. Post-Classification Assessment

The proposed RF_WT model outperformed baseline classifiers across most classes (Table 4). RF_WT achieved the highest F1-scores for bare land (0.896), forest

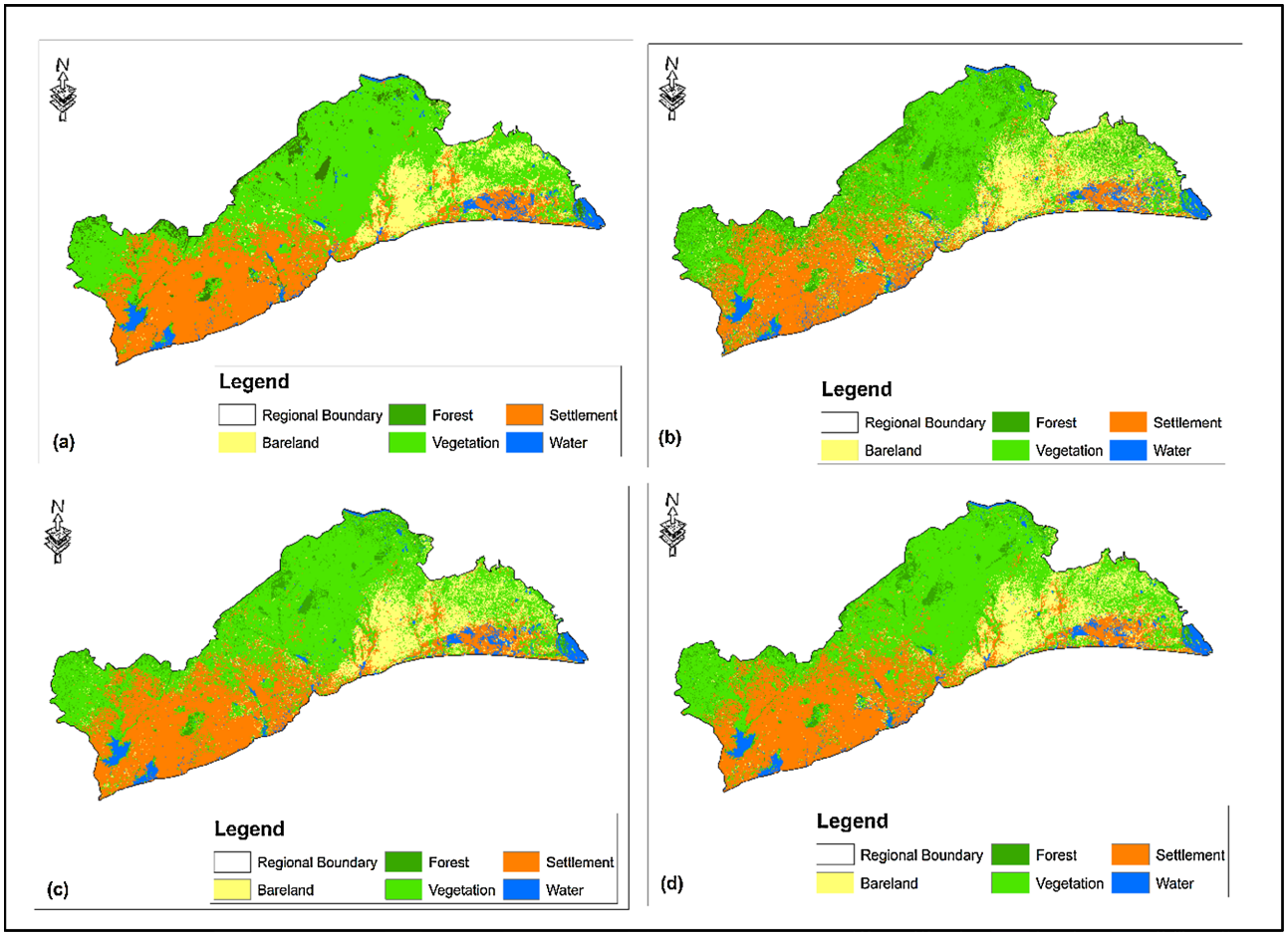

Figure 4. (a) Random Forest Wavelet Transform (RF_WT) filtered map showing post-processed output with enhanced spatial coherence, (b) Decision Tree (DT), (c) Gradient Boosting Machine (GBM), and (d) Random Forest (RF) classified maps.

Table 4. Post classification assessment.

Model	Metric	Land Cover Classes				
		Bareland	Forest	Vegetation	Settlement	Water
RF	UA	0.952	0.867	0.75	0.797	0.955
	PA	0.8	0.78	0.9	**0.94**	**0.84**
	F1	0.87	0.821	0.818	0.862	0.894
DT	UA	0.889	0.731	0.679	**0.87**	0.907
	PA	0.8	0.76	0.76	**0.94**	0.78
	F1	0.842	0.745	0.717	**0.904**	0.839
GBM	UA	0.949	0.86	0.719	0.783	0.932
	PA	0.74	0.74	0.92	**0.94**	0.82
	F1	0.831	0.796	0.807	0.855	0.872
RF_WT	UA	**0.935**	**0.909**	**0.847**	0.712	**0.976**
	PA	**0.86**	**0.8**	**0.999**	0.84	0.82
	F1	**0.896**	**0.851**	**0.917**	0.771	0.891

(0.851), vegetation (0.917), and water (0.891). Vegetation mapping showed the most pronounced improvement, with RF_WT reaching perfect producer's accuracy (0.999). In contrast, settlement classification remained more challenging, with RF_WT (F1 = 0.771) underperforming relative to RF (F1 = 0.862) and DT (F1 = 0.904). When summarised across all classes, RF_WT achieved the highest macro-averaged accuracy values (UA = 0.876, PA = 0.864, F1 = 0.865), compared with RF (UA = 0.864, PA = 0.852, F1 = 0.853), GBM (UA = 0.849, PA = 0.832, F1 = 0.832), and DT (UA = 0.815, PA = 0.808, F1 = 0.809). These results confirm the overall superiority of RF_WT in balancing omission and commission errors across natural land cover types. The comparison of the model performances by metric per land cover class are presented in Figures 5-7.

Figure 5. Comparison of model performance (user accuracy) per land cover class.

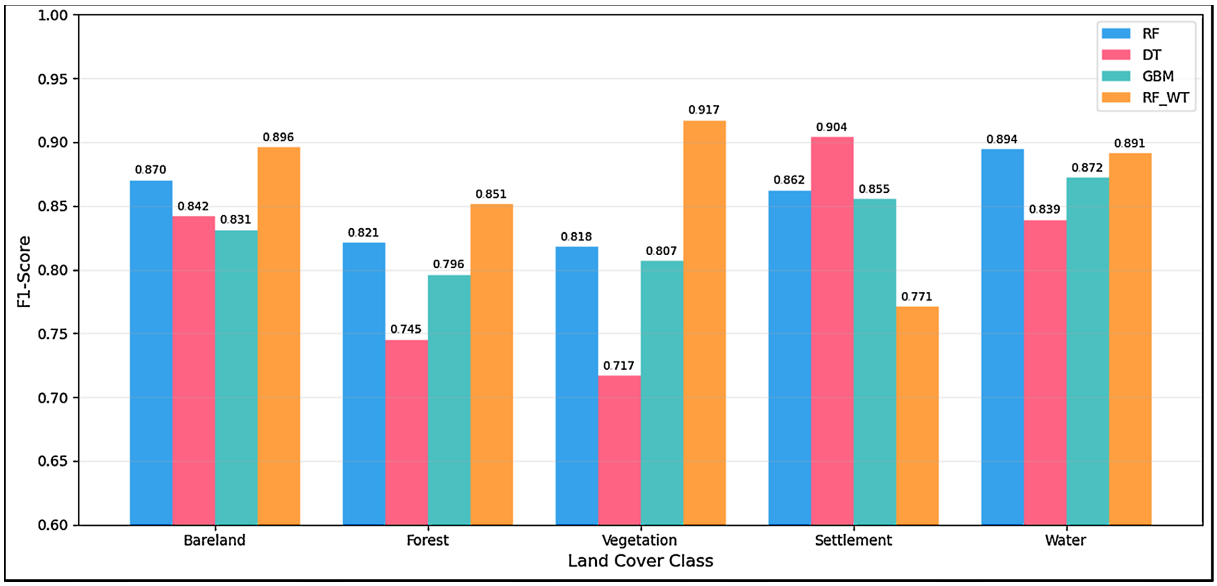

Figure 6. Comparison of model performance (producer accuracy) per land cover class.

Figure 7. Comparison of model performance (F1-score) per land cover class.

4. Discussion

The quantitative and qualitative results demonstrate that integrating a one-dimensional wavelet transform into a pixel-based workflow significantly improves the discriminative capability of the machine learning model for land-cover mapping from multispectral imagery. The proposed Random Forest Wavelet Transform (RF_WT) model outperformed other machine learning models trained on raw bands alone for most classes. These gains confirm that exposing both low-frequency trends and high-frequency detail in each spectral vector yields a richer, more discriminative feature space than raw reflectance alone. Per class-level outcomes, it is observed that improvements were largest for Vegetation (F1 = 0.917; PA = 0.999), followed by Bare land, Forest, and Water, where RF_WT attained the best or near-best F1. In contrast, Settlement remained comparatively difficult for RF_WT (F1 = 0.771), underperforming RF and DT trained on raw bands. The lower UA (0.712) suggests commission errors where spectrally mixed pixels at 30 m (impervious-vegetation-shadow) were labelled as settlement. This underlines a known limitation of medium-resolution optical data in heterogeneous urban areas.

Additionally, the classified maps reinforce the metrics. The RF_WT filtered map presented the most spatially coherent output, with compact, contiguous patches of vegetation and forest, clear water boundaries, and noticeable reduction of salt-and-pepper artefacts. The DT map was visibly fragmented; GBM showed mixing of settlement and vegetation in transitional zones; and baseline RF, although cleaner than DT and GBM, still exhibited more speckle and less compact settlement boundaries than RF_WT. The visual inspection thus corroborates the quantitative advantage of the wavelet-enhanced features combined with majority filtering.

The outstanding performance of the RF_WT model can be directly attributed to the complementary information provided by the wavelet decomposition. The

application of a 1D-Discrete Wavelet Transform to each pixel's spectral signature effectively separated the signal into distinct frequency components, allowing the classifier to access a richer and more physically interpretable feature set. The explainable AI (xAI) analyses, Gini importance, permutation importance, and SHAP values, consistently demonstrated that the model relied on both raw spectral bands and their wavelet reconstructions (WTALL, WTED, WTTR). Gini importance highlighted strong contributions from wavelet families alongside visible bands (B3, B4), indicating that the model repeatedly split on both raw spectra and decomposed signals. Permutation importance, which tests out-of-sample reliance, shifted the emphasis further toward WTED (detail/edge) features, especially WTED_B5 (SWIR1) and WTED_B6 (SWIR2). This observation demonstrates that high-frequency information in SWIR materially supported generalisation. SHAP global values confirmed this complementarity: RAW and WTALL families were highly influential overall, while WTED and WTTR provided additional lift, especially for classes where subtle spectral–textural cues matter (vegetation vs. forest; bare land vs. settlement edges). This finding implies that the wavelet features did not simply replace the raw data but augmented it. Thus, it provided new and discriminative axes for separation.

The importance of high-frequency detail components (WTED), particularly in the Short-Wave Infrared (SWIR1, Band 5) and visible regions, underscores how wavelet decomposition addresses fundamental challenges in pixel-based classification. The WTED_B5 feature, identified as highly important by permutation importance, captures fine-scale spectral variations and abrupt transitions within a pixel's spectral profile. These high-frequency details are often associated with material-specific absorption features and textural nuances that are smoothed over in the raw spectral signal or the low-frequency trend (WTTR). For natural classes like Vegetation, for which RF_WT achieved a near-perfect Producer's Accuracy (0.999), the wavelet features likely enhanced the separation of different vegetation health states and species by isolating subtle signal variations in the SWIR region, which are crucial for chlorophyll and water content assessment. Similarly, the improvement in Bareland classification (F1-score of 0.896) suggests that the detail components helped distinguish between different soil types, moisture levels, and geological features by amplifying their unique spectral textures.

Furthermore, the low-frequency approximation components (WTTR) provided a stabilising influence by representing the overarching spectral trend of a pixel. This likely helped reduce the impact of intra-class spectral variability and noise, a known challenge in medium-resolution imagery. By separating the general material, captured by WTTR, from the specific condition or texture, captured by WTED, the model could make more robust decisions. This dual capability explains the significant performance gains for heterogeneous natural classes, effectively addressing the issue of intra-class spectral variability highlighted by [42].

The present findings align with and extend the findings of previous studies that utilised feature decomposition for hyperspectral image (HSI) analysis. [19] demon-

strated that decomposing HSI data into trends and oscillations using 2D-Singular Spectrum Analysis (SSA) effectively suppressed noise, enhanced feature discriminability and improved classification. The present study echoes that the core principle of signal decomposition, which involves isolating information at different frequencies, is equally powerful and transferable to multispectral data. While Landsat-8 has fewer spectral bands than hyperspectral sensors, the wavelet transform proved adept at unlocking latent information within each band's spectral vector, moving beyond the limitations of using raw reflectance values alone.

This study also addresses the challenge of managing intra-class spectral variability via stratified approaches. For example, while [42] adapted endmember sets to local variability for impervious mapping, the proposed approach can be viewed as a form of feature-level stratification. Unlike geographical stratification, which partitions the study area into distinct spatial regions, or spectral mixture analysis, which adapts endmember sets based on pixel composition, the proposed feature-level stratification stratifies the information content within each pixel's spectral signal prior to classification. Thus, by decomposing the signal into pre-isolated frequency components (low-frequency trend and high-frequency detail), the proposed approach effectively created a stratified feature space where the classifier could learn decision rules specific to both broad spectral trends and fine-scale details. This eliminated the need for the model to implicitly learn this decomposition through signal decomposition without requiring spatial segmentation or endmember modelling. This process led to more efficient and accurate learning, particularly for classes with diverse spectral manifestations.

Notwithstanding the overall improvement, the RF_WT model performed less effectively than the baseline RF and DT models in identifying settlements (F1 = 0.771). This setback can be attributed to the limits of medium-resolution imagery for urban environments. A single Landsat pixel often contains multiple materials (e.g., roofing, asphalt, vegetation), resulting in a composite spectral signature that is highly variable and not easily characterised by spectral frequency alone. Consequently, the observed performance may suggest that wavelet-derived features inadvertently amplified the spectral confusion inherent in these mixed urban pixels. Thus, while the detail components (WTED) enhanced discrimination for homogeneous classes, these signals may have captured noise from the random multiple materials associated with heterogeneous settlement classes rather than a coherent "edge" signature. This noise introduced inconsistency, making it challenging for the RF_WT model and leading to misclassification. In comparison, the simpler spectral response in raw bands provides consistent spectral signatures, although limited, for classification.

Moreover, although wavelet decomposition enhances spectral discrimination, it does not explicitly capture spatial context or geometric patterns that are vital for urban classification. This finding is consistent with [43], who emphasised that accurate settlement mapping often requires integrating multi-source data to capture its multifaceted nature. Therefore, the lower performance for settlements high-

lights a key limitation of a purely spectral, pixel-based approach, even when enhanced with advanced signal processing.

5. Conclusion and Future Works

This study presented an approach to improve the accuracy and interpretability of land cover classification by integrating signal decomposition into a supervised machine learning framework. A Random Forest model enhanced with wavelet-derived features (RF_WT) was developed and evaluated against baseline models trained on raw spectral bands (RF, DT, GBM). The approach was designed to exploit the discriminative potential of low-frequency and high-frequency components extracted from each spectral vector. Notably, RF_WT substantially improved vegetation classification, achieving perfect producer's accuracy and the highest F1-score (0.917), while also providing gains in the bare land, forest, and water classes. These improvements confirm that wavelet decomposition enriches the spectral feature space, enabling the model to capture subtle variations that conventional classifiers often overlook. In addition, the integration of explainable AI metrics (Gini, permutation, SHAP) confirmed the complementary role of both raw and decomposed features, with wavelet-derived detail and trend components making a significant contribution to discrimination in the visible and SWIR bands.

Despite these advances, the classification of settlements remained challenging, with RF_WT underperforming relative to the baseline RF and DT models. This shortcoming reflects the intrinsic spectral heterogeneity of urban pixels at Landsat resolution, where the detection of fine-scale urban features is limited and subtle spectral variations crucial for identifying built-up classes are suppressed. The result highlights a key limitation of the approach: while decomposition improves natural class separability, it does not fully resolve the complexity of built-up areas.

Future studies could focus on improving settlement classification by integrating texture descriptors, object-based analysis, or morphological features that capture spatial context beyond pixel-level spectral information. Additionally, the framework could be tested with higher-resolution imagery (e.g., Sentinel-2, PlanetScope, or WorldView), leverage multi-source information (e.g., SAR, nighttime lights, DEM), and incorporate temporal dynamics to assess class separability in heterogeneous landscapes. Also, the performance of other signal decomposition techniques can be assessed while accounting for the effect of class imbalance.

Acknowledgements

The authors wish to thank the management of the University of Mines and Technology (UMaT) and the Department of Geomatic Engineering for allowing the use of their GIS laboratory to process and analyse data for this research.

Conflicts of Interest

The authors declare no conflicts of interest regarding the publication of this paper.

References

[1] Navin, M.S. and Agilandeeswari, L. (2020) Comprehensive Review on Land Use/Land Cover Change Classification in Remote Sensing. *Journal of Spectral Imaging*, **9**, a8.

[2] Ramachandra, T.V., Mondal, T. and Setturu, B. (2023) Relative Performance Evaluation of Machine Learning Algorithms for Land Use Classification Using Multispectral Moderate Resolution Data. *SN Applied Sciences*, **5**, Article 274. https://doi.org/10.1007/s42452-023-05496-4

[3] Ali, U., Esau, T.J., Farooque, A.A., Zaman, Q.U., Abbas, F. and Bilodeau, M.F. (2022) Limiting the Collection of Ground Truth Data for Land Use and Land Cover Maps with Machine Learning Algorithms. *ISPRS International Journal of Geo-Information*, **11**, Article 333. https://doi.org/10.3390/ijgi11060333

[4] Barman, P., Mustak, S., Kuffer, M. and Singh, S.K. (2023) Transfer-Ensemble Learning: A Novel Approach for Mapping Urban Land Use/Cover of the Indian Metropolitans. *Sustainability*, **15**, Article 16593. https://doi.org/10.3390/su152416593

[5] Qin, R. and Liu, T. (2022) A Review of Landcover Classification with Very-High Resolution Remotely Sensed Optical Images—Analysis Unit, Model Scalability and Transferability. *Remote Sensing*, **14**, Article 646. https://doi.org/10.3390/rs14030646

[6] Shimabukuro, Y.E., Arai, E., da Silva, G.M., Hoffmann, T.B., Duarte, V., Martini, P.R., *et al.* (2023) Mapping Land Use and Land Cover Classes in São Paulo State, Southeast of Brazil, Using Landsat-8 OLI Multispectral Data and the Derived Spectral Indices and Fraction Images. *Forests*, **14**, Article 1669. https://doi.org/10.3390/f14081669

[7] Talukdar, S., Singha, P., Mahato, S., Shahfahad,, Pal, S., Liou, Y., *et al.* (2020) Land-use Land-Cover Classification by Machine Learning Classifiers for Satellite Observations—A Review. *Remote Sensing*, **12**, Article 1135. https://doi.org/10.3390/rs12071135

[8] Li, R., Zheng, S., Duan, C., Wang, L. and Zhang, C. (2022) Land Cover Classification from Remote Sensing Images Based on Multi-Scale Fully Convolutional Network. *Geo-spatial Information Science*, **25**, 278-294. https://doi.org/10.1080/10095020.2021.2017237

[9] Huang, C., Davis, L.S. and Townshend, J.R.G. (2002) An Assessment of Support Vector Machines for Land Cover Classification. *International Journal of Remote Sensing*, **23**, 725-749. https://doi.org/10.1080/01431160110040323

[10] Nguyen, H.T.T., Doan, T.M. and Radeloff, V. (2018) Applying Random Forest Classification to Map Land Use/Land Cover Using Landsat 8 Oli. *The International Archives of the Photogrammetry, Remote Sensing and Spatial Information Sciences*, **3**, 363-367. https://doi.org/10.5194/isprs-archives-xlii-3-w4-363-2018

[11] Madarasinghe, S.K., Yapa, K.K.A.S. and Jayatissa, L.P. (2020) Google Earth Imagery Coupled with On-Screen Digitization for Urban Land Use Mapping: Case Study of Hambantota, Sri Lanka. *Journal of the National Science Foundation of Sri Lanka*, **48**, 357-366. https://doi.org/10.4038/jnsfsr.v48i4.9795

[12] Gómez, C., White, J.C. and Wulder, M.A. (2016) Optical Remotely Sensed Time Series Data for Land Cover Classification: A Review. *ISPRS Journal of Photogrammetry and Remote Sensing*, **116**, 55-72. https://doi.org/10.1016/j.isprsjprs.2016.03.008

[13] Belgiu, M. and Drăguţ, L. (2016) Random Forest in Remote Sensing: A Review of Applications and Future Directions. *ISPRS Journal of Photogrammetry and Remote Sensing*, **114**, 24-31. https://doi.org/10.1016/j.isprsjprs.2016.01.011

[14] Abdi, A.M. (2019) Land Cover and Land Use Classification Performance of Machine

Learning Algorithms in a Boreal Landscape Using Sentinel-2 Data. *GIScience & Remote Sensing*, **57**, 1-20. https://doi.org/10.1080/15481603.2019.1650447

[15] Rodriguez-Galiano, V.F., Ghimire, B., Rogan, J., Chica-Olmo, M. and Rigol-Sanchez, J.P. (2012) An Assessment of the Effectiveness of a Random Forest Classifier for Land-Cover Classification. *ISPRS Journal of Photogrammetry and Remote Sensing*, **67**, 93-104. https://doi.org/10.1016/j.isprsjprs.2011.11.002

[16] Fu, H., Sun, G., Ren, J., Zhang, A. and Jia, X. (2022) Fusion of PCA and Segmented-PCA Domain Multiscale 2-D-SSA for Effective Spectral-Spatial Feature Extraction and Data Classification in Hyperspectral Imagery. *IEEE Transactions on Geoscience and Remote Sensing*, **60**, 1-14. https://doi.org/10.1109/tgrs.2020.3034656

[17] Shih, H., Stow, D.A. and Tsai, Y.H. (2018) Guidance on and Comparison of Machine Learning Classifiers for Landsat-Based Land Cover and Land Use Mapping. *International Journal of Remote Sensing*, **40**, 1248-1274. https://doi.org/10.1080/01431161.2018.1524179

[18] Signoroni, A., Savardi, M., Baronio, A. and Benini, S. (2019) Deep Learning Meets Hyperspectral Image Analysis: A Multidisciplinary Review. *Journal of Imaging*, **5**, Article 52. https://doi.org/10.3390/jimaging5050052

[19] Zabalza, J., Ren, J., Zheng, J., Han, J., Zhao, H., Li, S., *et al.* (2015) Novel Two-Dimensional Singular Spectrum Analysis for Effective Feature Extraction and Data Classification in Hyperspectral Imaging. *IEEE Transactions on Geoscience and Remote Sensing*, **53**, 4418-4433. https://doi.org/10.1109/tgrs.2015.2398468

[20] Fu, H., Sun, G., Ren, J., Zabalza, J., Zhang, A. and Yao, Y. (2020) 2D-SSA Based Multiscale Feature Fusion for Feature Extraction and Data Classification in Hyperspectral Imagery. *IGARSS* 2020—2020 *IEEE International Geoscience and Remote Sensing Symposium*, Waikoloa, 26 September-2 October 2020, 76-79. https://doi.org/10.1109/igarss39084.2020.9323776

[21] Kang, X., Duan, P. and Li, S. (2020) Hyperspectral Image Visualization with Edge-Preserving Filtering and Principal Component Analysis. *Information Fusion*, **57**, 130-143. https://doi.org/10.1016/j.inffus.2019.12.003

[22] Boamah Poku, M., Yakubu, I., Yevenyo Ziggah, Y., Poku, M.B., Yakubu, I. and Ziggah, Y.Y. (2023) Assessing the Performance of Machine Learning Algorithms for Urban Land Cover Classification using Multispectral Satellite Imagery. *Ghana Journal of Technology*, **7**, 10-18.

[23] Phan, T.N., Kuch, V. and Lehnert, L.W. (2020) Land Cover Classification Using Google Earth Engine and Random Forest Classifier—The Role of Image Composition. *Remote Sensing*, **12**, Article 2411. https://doi.org/10.3390/rs12152411

[24] Tassi, A., Gigante, D., Modica, G., Di Martino, L. and Vizzari, M. (2021) Pixel- vs. Object-Based Landsat 8 Data Classification in Google Earth Engine Using Random Forest: The Case Study of Maiella National Park. *Remote Sensing*, **13**, Article 2299. https://doi.org/10.3390/rs13122299

[25] Vermote, E., Justice, C., Claverie, M. and Franch, B. (2016) Preliminary Analysis of the Performance of the Landsat 8/OLI Land Surface Reflectance Product. *Remote Sensing of Environment*, **185**, 46-56. https://doi.org/10.1016/j.rse.2016.04.008

[26] Gorelick, N., Hancher, M., Dixon, M., Ilyushchenko, S., Thau, D. and Moore, R. (2017) Google Earth Engine: Planetary-Scale Geospatial Analysis for Everyone. *Remote Sensing of Environment*, **202**, 18-27. https://doi.org/10.1016/j.rse.2017.06.031

[27] Bwangoy, J.B., Hansen, M.C., Roy, D.P., Grandi, G.D. and Justice, C.O. (2010) Wetland Mapping in the Congo Basin Using Optical and Radar Remotely Sensed Data

and Derived Topographical Indices. *Remote Sensing of Environment*, **114**, 73-86. https://doi.org/10.1016/j.rse.2009.08.004

[28] de Sousa, C., Fatoyinbo, L., Neigh, C., Boucka, F., Angoue, V. and Larsen, T. (2020) Cloud-computing and Machine Learning in Support of Country-Level Land Cover and Ecosystem Extent Mapping in Liberia and Gabon. *PLOS ONE*, **15**, e0227438. https://doi.org/10.1371/journal.pone.0227438

[29] Dong, J., Xiao, X., Sheldon, S., Biradar, C., Duong, N.D. and Hazarika, M. (2012) A Comparison of Forest Cover Maps in Mainland Southeast Asia from Multiple Sources: PALSAR, MERIS, MODIS and Fra. *Remote Sensing of Environment*, **127**, 60-73. https://doi.org/10.1016/j.rse.2012.08.022

[30] Hansen, M.C., Roy, D.P., Lindquist, E., Adusei, B., Justice, C.O. and Altstatt, A. (2008) A Method for Integrating MODIS and Landsat Data for Systematic Monitoring of Forest Cover and Change in the Congo Basin. *Remote Sensing of Environment*, **112**, 2495-2513. https://doi.org/10.1016/j.rse.2007.11.012

[31] Midekisa, A., Holl, F., Savory, D.J., Andrade-Pacheco, R., Gething, P.W., Bennett, A., *et al.* (2017) Mapping Land Cover Change over Continental Africa Using Landsat and Google Earth Engine Cloud Computing. *PLOS ONE*, **12**, e0184926. https://doi.org/10.1371/journal.pone.0184926

[32] Cohen, A. and Kovacevic, J. (1996) Wavelets: The Mathematical Background. *Proceedings of the IEEE*, **84**, 514-522. https://doi.org/10.1109/5.488697

[33] C., E.W. and Daubechies, I. (1993) Ten Lectures on Wavelets. *Mathematics of Computation*, **61**, 941-942. https://doi.org/10.2307/2153268

[34] Mallat, S.G. (2009) A Theory for Multiresolution Signal Decomposition: The Wavelet Representation. In: Heil, C. and Walnut, D.F., Eds., *Fundamental Papers in Wavelet Theory*, Princeton University Press, 494-513. https://doi.org/10.1515/9781400827268.494

[35] Prabhu, N., Arora, M.K. and Balasubramanian, R. (2016) Wavelet Based Feature Extraction Techniques of Hyperspectral Data. *Journal of the Indian Society of Remote Sensing*, **44**, 373-384. https://doi.org/10.1007/s12524-015-0506-9

[36] Quinlan, J.R. (1986) Induction of Decision Trees. *Machine Learning*, **1**, 81-106. https://doi.org/10.1023/a:1022643204877

[37] Breiman, L. (2001) Random Forests. *Machine Learning*, **45**, 5-32. https://doi.org/10.1023/a:1010933404324

[38] Friedman, J.H. (2001) Greedy Function Approximation: A Gradient Boosting Machine. *The Annals of Statistics*, **29**, 1189-1232. https://doi.org/10.1214/aos/1013203451

[39] Dorogush, A., Ershov, V. and Gulin, A. (2018) CatBoost: Unbiased Boosting with Categorical Features. 32*nd Conference on Neural Information Processing Systems* (*NeurIPS* 2018), Montréal, 2-8 December 2018, 6638-6648.

[40] Ke, G., Meng, Q., Finley, T., Wang, T., Chen, W., Ma, W., Ye, Q. and Liu, T.Y. (2017) LightGBM: A Highly Efficient Gradient Boosting Decision Tree. 31*st Conference on Neural Information Processing Systems* (*NIPS* 2017), Long Beach, 4-9 December 2017, 3147-3155.

[41] Nsiah, R.A., Mantey, S. and Ziggah, Y.Y. (2024) Assessing the Contribution of RGB Vis in Improving Building Extraction from RGB-UAV Images. *Mersin Photogrammetry Journal*, **6**, 9-21. https://doi.org/10.53093/mephoj.1399083

[42] Ji, H., Li, X., Wei, X., Liu, W., Zhang, L. and Wang, L. (2020) Mapping 10-M Resolution Rural Settlements Using Multi-Source Remote Sensing Datasets with the Google

Earth Engine Platform. *Remote Sensing*, **12**, Article 2832. https://doi.org/10.3390/rs12172832

[43] Sun, G., Chen, X., Ren, J., Zhang, A. and Jia, X. (2017) Stratified Spectral Mixture Analysis of Medium Resolution Imagery for Impervious Surface Mapping. *International Journal of Applied Earth Observation and Geoinformation*, **60**, 38-48. https://doi.org/10.1016/j.jag.2017.04.006